GENERAL RELATIVISTIC SIMULATIONS OF MAGNETIZED PLASMAS AROUND MERGING SUPERMASSIVE BLACK HOLES

BRUNO GIACOMAZZO,[1,2,3] JOHN G. BAKER,[3] M. COLEMAN MILLER,[2,4] CHRISTOPHER S. REYNOLDS,[2,4] JAMES R. VAN METER,[3]

Draft version March 26, 2012

ABSTRACT

Coalescing supermassive black hole binaries are produced by the mergers of galaxies and are the most powerful sources of gravitational waves accessible to space-based gravitational observatories. Some such mergers may occur in the presence of matter and magnetic fields and hence generate an electromagnetic counterpart. In this paper we present the first general relativistic simulations of magnetized plasma around merging supermassive black holes using the general relativistic magnetohydrodynamic code Whisky. By considering different magnetic field strengths, going from non-magnetically dominated to magnetically dominated regimes, we explore how magnetic fields affect the dynamics of the plasma and the possible emission of electromagnetic signals. In particular we observe a total amplification of the magnetic field of ~ 2 orders of magnitude which is driven by the accretion onto the binary and that leads to stronger electromagnetic signals than in the force-free regime where such amplifications are not possible.

Keywords: accretion, accretion disks — black hole physics — gravitational waves — magnetohydrodynamics (MHD) — methods: numerical

1. INTRODUCTION

Space-based gravitational-wave detectors, such as the planned eLISA/NGO and SGO detectors, are expected to detect tens of supermassive black hole mergers per year. These detections will provide superbly precise measurements of the redshifted masses of the holes as well as the luminosity distance to the event. However, it is not possible to extract the redshift directly from the gravitational waves. For this it is necessary to look for electromagnetic signatures that would identify the host galaxy. The resulting combination of the redshift with the luminosity distance would provide a powerful cosmological probe (Hughes & Holz 2003; Berti et al. 2005; Kocsis et al. 2006; Arun et al. 2009). It would also allow precise tests of whether gravitons travel at the speed of light, as required by general relativity. Although the merger itself produces no electromagnetic emission, if there are significant electromagnetic fields or mass nearby in an accretion disk then there are various possibilities. For some disk accretion rates and binary mass ratios, the binary reaches a point in its coalescence such that further inspiral by emission of gravitational waves occurs more rapidly than the disk diffuses inwards (Milosavljević & Phinney 2005). This leads to a hole in the disk which is filled gradually after merger, leading to a source that brightens over weeks to years depending on various parameters (Milosavljević & Phinney 2005; Krolik 2010; Tanaka & Menou 2010; Shapiro 2010). Several authors have discussed consequences of the recoils from asymmetric emission of gravitational waves during the coalescence, from prompt shocks to delayed emission lasting millions of years (Shields & Bonning 2008; Megevand et al. 2009; Lippai et al. 2008; Corrales et al. 2010; Anderson et al. 2010; Rossi et al. 2010; Zanotti et al. 2010). Emission might occur in the late inspiral from effects such as enhanced accretion, periodic Newtonian perturbations, or shearing of the disk due to gravitational waves (Kocsis & Loeb 2008; Schnittman & Krolik 2008). Earlier precursors are also possible, and in some cases the error volume from the gravitational wave signal may be small enough that the host galaxy can be identified by morphology, mass, or by the presence of an AGN.

In the last few years there have been a number of publications describing the evolution of gas and magnetic fields around merging supermassive black holes. Van Meter and collaborators performed test-particle simulations of the motion of accreting gas during the last phase of inspiral of comparable-mass supermassive black holes (van Meter et al. 2010). These simulations suggested that near merger a significant fraction of particles can collide with each other at speeds approaching the speed of light, implying that a burst of radiation might accompany the coalescence. Other works have instead started to investigate the effect that the merging black holes (BHs) would have on surrounding gas and the possible emission of EM signals (O'Neill et al. 2009; Farris et al. 2010; Farris et al. 2011; Bode et al. 2010; Bogdanović et al. 2011; Bode et al. 2012). At the same time there have been the first investigations of the effect of binary black hole (BBH) mergers on electromagnetic fields in vacuum (Palenzuela et al. 2009, 2010c; Mösta et al. 2010) and in a magnetically dominated plasma (Palenzuela et al. 2010b,a; Mösta et al. 2011).

These studies have shown how magnetic and electric fields can be distorted by the motion of the BHs and hence lead to possible electromagnetic emission. In particular, recent studies by Palenzuela and Mösta (Palenzuela et al. 2010b,a; Mösta et al. 2011) have raised the possibility that the motion of two BHs in a magnetically dominated plasma, i.e., in the so called force-free regime, could generate two separate jets, one around each BH, during the inspiral. At the time of the merger these two collimated jets would enter in contact and form a single jet emitted from the spinning BH formed after the merger. It is, however, still unknown how general this scenario is and whether the emission would be detectable.

[1] JILA, University of Colorado, 440 UCB, Boulder, CO 80309, USA
[2] Department of Astronomy, University of Maryland, College Park, MD 20742, USA
[3] Gravitational Astrophysics Laboratory, NASA Goddard Space Flight Center, Greenbelt, MD 21114, USA
[4] Joint Space Science Institute, University of Maryland, College Park, MD 20742, USA

In this paper we present the first results from general relativistic magnetohydrodynamic (GRMHD) simulations of magnetized plasmas around merging supermassive black holes. By considering the evolution of equal-mass BBH systems in plasmas with different levels of magnetization we fill the gap between the studies of non-magnetized gas and the results obtained in the force-free and electro-vacuum regimes. We use a spacelike signature $(-, +, +, +)$ and will typically use a system of units in which $c = G = M = 1$, where M is the total mass of the binary. In these units $1\,M$ is equivalent to $\sim 0.14\,M_8$ hours and to $\sim 4.86 \times 10^{-6}\,M_8$ pc, where $M_8 \equiv M/(10^8 M_\odot)$.

2. NUMERICAL METHODS AND INITIAL DATA

Most of the details on the mathematical and numerical setup used for producing the results presented here are discussed in depth elsewhere (Pollney et al. 2007; Thornburg 2004; Giacomazzo & Rezzolla 2007; Giacomazzo et al. 2009, 2011; Löffler et al. 2011). In what follows, we limit ourselves to a brief overview.

2.1. Magnetohydrodynamics and Einstein equations

The evolution of the spacetime was obtained using the Ccatie code, a three-dimensional finite-differencing code providing the solution of a conformal traceless formulation of the Einstein equations (Pollney et al. 2007), and we used the "moving puncture" method and gauge conditions developed in van Meter et al. 2006. The GRMHD equations were instead solved using the Whisky code (Giacomazzo & Rezzolla 2007; Giacomazzo et al. 2011), which adopts a flux-conservative formulation of the equations as presented in Antón et al. (2006) and high-resolution shock-capturing schemes (HRSC). All the results presented here have been computed using the Piecewise Parabolic Method (PPM) (Colella & Woodward 1984), while the Harten-Lax-van Leer-Einfeldt (HLLE) approximate Riemann solver (Harten et al. 1983) has been used to compute the fluxes. All the simulations were performed using a polytropic equation of state (EOS) with a polytropic exponent $\gamma = 4/3$ and a polytropic constant $\kappa = 0.2$. The use of a polytropic EOS instead of the more common ideal-fluid EOS was done mainly because of numerical robustness and performance. The use instead of an ideal-fluid EOS would not affect the main results of this work.

In order to guarantee the divergence-free character of the MHD equations we have employed the flux-CD approach described in Toth (2000), but with one substantial difference, namely, that we use as an evolution variable the vector potential instead of the magnetic field. In other words, by using an expression similar to equation (31) of Toth (2000), we compute the electric field at the center of each numerical cell by interpolating the fluxes computed at the interfaces of the cell and then use it to evolve directly the vector potential (Giacomazzo et al. 2011; Rezzolla et al. 2011). When evolving the vector potential a gauge choice needs to be made and we here use the "algebraic gauge" (Etienne et al. 2012) which was also used in previous GRMHD simulations with the Whisky code (Giacomazzo et al. 2011; Rezzolla et al. 2011). The code has been validated against a series of tests in special relativity (Giacomazzo & Rezzolla 2006) and in full general relativity (Giacomazzo & Rezzolla 2007).

Since the simulations performed here consider a plasma with a total mass negligible with respect to the mass of the two black holes, we have decoupled the Einstein equations from the matter dynamics, i.e., the metric variables are evolved using Einstein equations in vacuum. The same was done in the general relativistic hydrodynamic simulations reported in Farris et al. (2010). Moreover, in order to prevent the formation of nonphysical values in the MHD quantities, we have excised the MHD variables inside the apparent horizon of each BH.

2.2. Adaptive Mesh Refinements

Both the Einstein and the GRMHD equations are solved using the vertex-centered adaptive mesh-refinement (AMR) approach provided by the Carpet driver (Schnetter et al. 2004). Our rather basic form of AMR consists of centering the highest-resolution level around each black hole and in moving the "boxes" following the position of the two BHs. For the results presented here we have used 11 refinement levels with the finest resolution being $0.0375M$ and the coarsest resolution being $38.4M$. The finest grid has a radius of $6M$ whereas the coarsest grid extends to $1536M$. The large extent of our finest grid allows us to follow accurately the dynamics of the plasma around the BHs and it is also sufficiently large to avoid the spurious magnetic field amplifications that may occur when evolving the vector potential with the "algebraic gauge" (Etienne et al. 2012).

For all the simulations reported here we have also used a reflection-symmetry condition across the $z = 0$ plane and a π-symmetry condition across the $x = 0$ plane[5]. At the outer boundary we instead used simple zeroth-order extrapolation on the MHD variables (in practice, we just copy the value of the MHD quantities from the outermost evolved point in each direction to the points of the outer boundary in that direction).

The time evolution is carried out using a 4th-order-accurate Runge-Kutta integration algorithm. Boundary data for finer grids are calculated with spatial prolongation operators employing 3rd-order polynomials for the matter variables and 5th-order polynomials for the spacetime variables. The prolongation in time employs 2nd-order polynomials and this ensures a significant memory saving, requiring only three timelevels to be stored, with little loss of accuracy due to the long dynamical timescale relative to the typical grid timestep.

2.3. Initial Data

We have considered equal-mass systems of two non-spinning BHs with an initial separation of $4.24M$; these inspiral for approximately three orbits before merger. The initial data were computed using the public available TwoPuncture code developed in Ansorg et al. 2004 and we chose the momentum of the punctures in order to ensure that the orbit of the two BHs is quasicircular. We have considered two models: B0 is surrounded by a non-magnetized plasma, and model B2 instead has an initially uniform magnetic field with a ratio of magnetic to gas pressure $(p_{mag}/p_{gas} \equiv \beta^{-1})$ initially equal to 2.5×10^{-2}. The magnetic field is aligned with the total angular momentum of the system, i.e., $B^i = (0, 0, B^z)$ while in all the models the rest-mass density ρ is initially uniform and fills the entire domain; we have in mind a flow that could be advection-dominated close to the holes (e.g., Ichimaru 1977) and thus have a high enough radial velocity that it can keep up with the binary inspiral throughout the entire coalescence. The initial distribution of the magnetic field is similar to that adopted in previous works (Palenzuela

---

[5] Stated differently, we evolve only the region $\{x \geq 0,\, z \geq 0\}$ and apply a $180°$-rotational-symmetry boundary condition across the plane at $x = 0$.
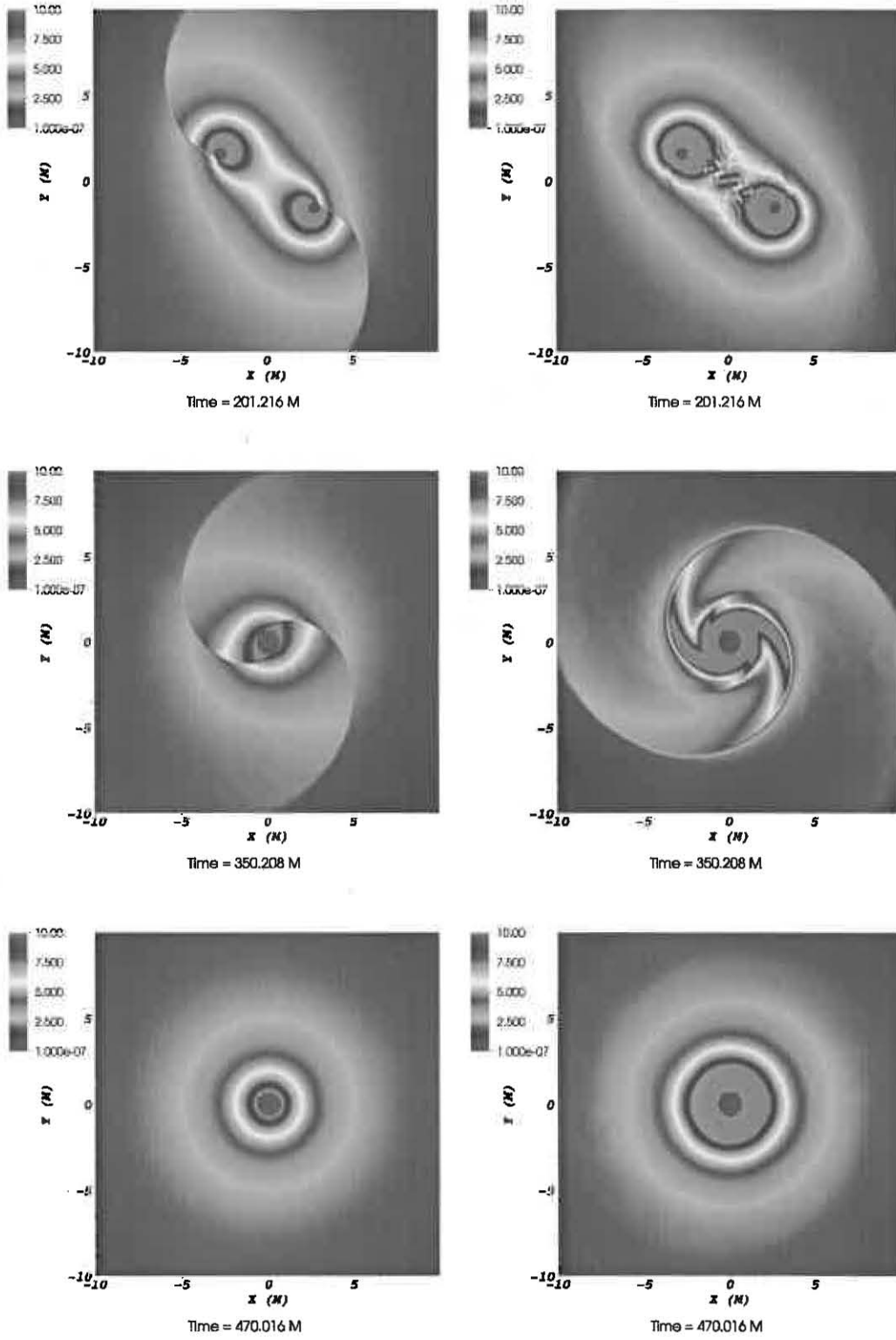
Figure 1. Evolution of the rest-mass density ρ on the equatorial plane for the non-magnetized model B0 (left panels) and for the magnetized case B2 (right panels). The units of time (shown at the bottom of each panel) and distance are M and the rest-mass density is normalized to its initial value.
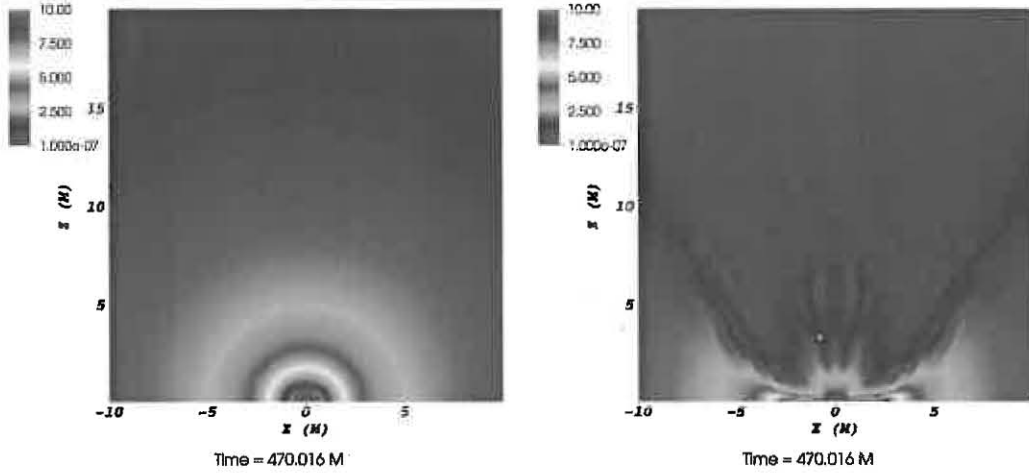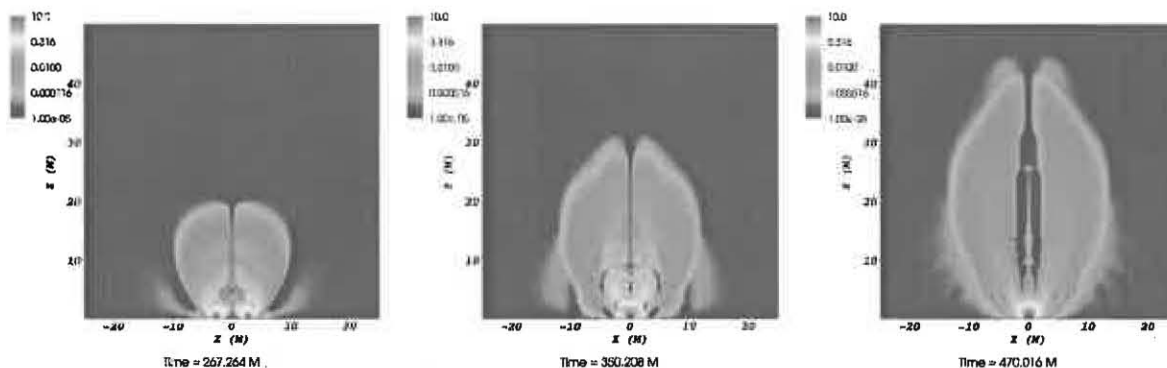
Figure 2. Rest-mass density ρ on the xz plane for the non-magnetized model B0 (left panel) and for the magnetized case B2 (right panel) at the end of the simulation ($t \sim 470M$). The unit of distance is M and the rest-mass density is normalized to its initial value.
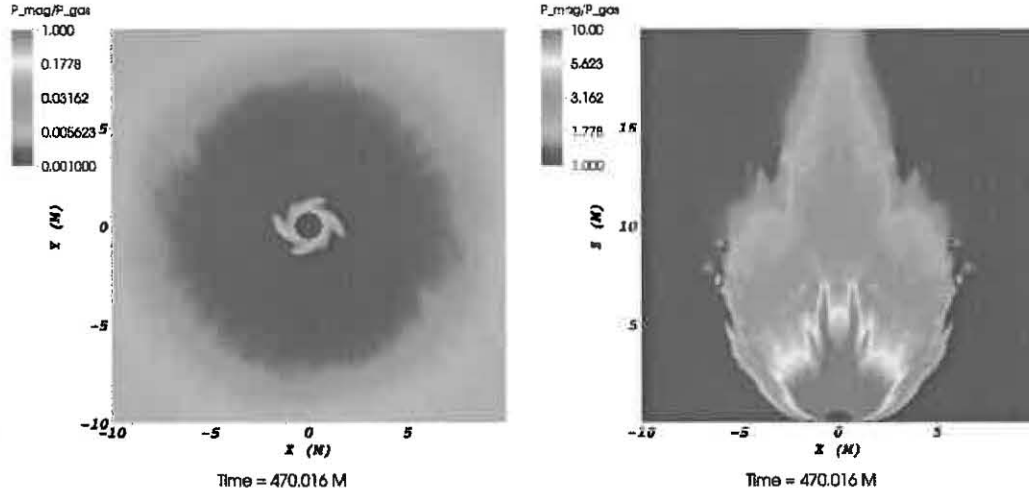
Figure 3. Ratio of magnetic to gas pressure for the magnetized model B2 on the xy (left panel) and xz planes (right panel) at the end of the simulation ($t \sim 470M$). The unit of distance is M. Note that the color bar is different between these two panels, on the left panel any magnetically dominated region would be in red while in the right panel the minimum value of the color bar is $p_{mag}/p_{gas} = 1$ in order to highlight only those regions that are magnetically dominated. The right panel contains five refinement levels; the finest refinement extends to $z = 6$ and the coarsest applies to $z = 14 - 20$.

Figure 4. Evolution of the Poynting vector on the xz plane for the magnetized model B2. The panels refer respectively to the time after two orbits, at the merger and at the end of the simulation. The units of time (shown at the bottom of each panel) and distance are M.

et al. 2010b,a; Mösta et al. 2011) and it assumes that the magnetic field is anchored to a circumbinary disk located far outside of the numerical domain.

3. DYNAMICS

Figure 1 shows the evolution of the rest-mass density ρ on the equatorial plane for models B0 (left panels) and B2 (right panels). The evolution of the non-magnetized model (left panels) resembles the one described in Farris et al. (2010) with the formation of two spiral shocks during the inspiral and the formation of a central spinning BH surrounded by a spherical distribution of matter accreting onto it. The magnetized model (right panels) shows quite different dynamics. During the evolution the magnetic field strength increases by approximately two orders of magnitude and contributes significantly to the total pressure in the gas. Because of this[6], the two shock waves that are present during the inspiral of model B0 are strongly reduced and hardly visible (first panel in the right column). Moreover, the density close to each of the two BHs and in the region connecting the two BHs is much larger than in the unmagnetized case. In this region it is also possible to see the formation of instabilities that are not present without magnetic fields. Soon after the merger (second panel in the right column) the spinning BH is surrounded by a disk with a density a factor of ~ 3 larger than in the unmagnetized case (see also discussion later in this section), and two shock waves are formed and the system finally relaxes to its final configuration (third panel in the right column). The temperature in the magnetic simulation is larger by up to $\sim 40\%$ for model B2 than in the unmagnetized model.

Although the evolution on the equatorial plane already shows some differences due to the effect of the magnetic field, the main difference is in the rest-mass density on the meridional plane. In Figure 2 we show the rest-mass density ρ on the xz plane for models B0 (left panel) and B2 (right panel) at the end of the simulation ($t \sim 470M$). Whereas the end result of the evolution of the unmagnetized model is a plasma accreting spherically onto a spinning BH, in the case of the magnetized model B2 the system forms a thin accretion disk and a funnel is created around the spin axis of the BH. Although at this time no relativistic jet is emitted (the Lorentz factor is lower than ~ 3 at the end of the simulation), such emission might exist at later times (which are outside the scope of the

present paper).

The difference between the rest-mass density distribution in the unmagnetized and magnetized cases can be better understood by looking at Figure 3, which shows the ratio of magnetic to gas pressure (i.e., the inverse of the plasma parameter β) for model B2 on the xy (left panel) and xz planes (right panel) at the end of the simulation ($t \sim 470M$). On the equatorial plane no region is magnetically dominated and the central region inside the disk has larger values of β than in the initial conditions, but the xz plane shows clearly the presence of a strongly magnetically dominated region close to the spin axis of the BH with $\beta \sim 10^{-2}$. This highly magnetized region is responsible for the creation of the thin disk and its funnel.

4. ELECTRO-MAGNETIC EMISSION

In figure 4 we show the evolution of the z component of the Poynting vector on the xz plane for model B2. We show in particular its outgoing component after two orbits (first panel), at the time of the merger (second panel) and at the end of the simulation (third panel). One of the main differences with respect to force-free simulations is that we do not observe the two strong and distinct jets originating from each black hole and the "jet" that is emitted by the system propagates slowly into the medium surrounding the binary. Whereas in the force-free scenarios the jet propagates in a very low-density medium where the inertia of the plasma can be neglected, in our simulations the jet has to break through the infalling medium outside the binary. We also note that in our scenario the emission is mainly collimated and parallel to the angular momentum of the binary and to the spin of the final BH with no sign of the dominant quadrupolar emission that was observed in the recent force-free simulations of Mösta et al. 2011.

Finally, in figure 5 we show the Poynting flux luminosity computed for model B2 (blue solid line). We have rescaled our results to consider a binary system with a total mass of $10^8 M_\odot$ and immersed in a plasma with a rest-mass density $\rho = 10^{-11} g\,cm^{-3}$. This corresponds to having an initial magnetic field of $\sim 10^4 G$ for model B2, which is also the same magnetic field strength considered in Palenzuela et al. (2010b). The luminosity is computed at a distance of $r_{ex} = 10M$. Model B2 shows the characteristic increase in luminosity during the inspiral, with a peak corresponding to the time of the merger, followed by a drop-off of a factor ~ 2. This is qualitatively similar to what is observed in force-free simulations (Palenzuela et al. 2010b), but our actual lu-

---

[6] See Mizuno et al. (2009) for an example of how the magnetic pressure can affect shock formation.
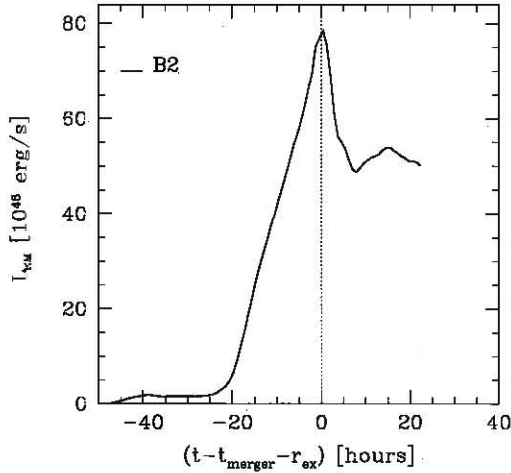
Figure 5. Evolution of the luminosity for the magnetized model B2 (blue solid line). The luminosity is computed at a distance $r_{ex} = 10M$ for a binary system with a total mass of $10^8 M_\odot$ and an initial rest-mass density of $10^{-11} g\ cm^{-3}$.

minosities are considerably higher. This happens because in our ideal GRMHD simulations the magnetic field is amplified of ∼ 2 orders of magnitude. So even when starting with a magnetic field of ∼ $10^4 G$, the final configuration has a field of ∼ $10^6 G$. If we were to compare with force-free simulations starting with such a high field we would obtain similar luminosities (Palenzuela et al. 2010b). Indeed we note that our luminosity at the end is ∼ $10^{47} erg\ s^{-1}$ and in the simulations reported in Palenzuela et al. 2010b is ∼ $10^{43} erg\ s^{-1}$ for a magnetic field that is ∼ 2 orders of magnitude lower than the one we have at the end of our simulations. Since the luminosity L_{EM} scales as B^2 our values are consistent with those one would observe in a force-free regime. This again highlights one of the main differences between our simulations and those assuming a force-free regime since the beginning. Because of the accretion of the plasma onto the BHs, magnetic field lines are compressed and twisted driving the large amplification we observe. In a force-free regime, the magnetic field is decoupled from the dynamics of the matter and such large amplifications cannot be obtained.

5. CONCLUSIONS

We have presented the first numerical GRMHD simulations of magnetized plasmas around merging supermassive binary black holes. We have for the first time investigated the role of magnetic fields in the plasma dynamics and filled the gap between the works that have considered non-magnetized gas and the results obtained in the force-free and electro-vacuum regimes.

We have shown that even plasmas that are initially not magnetically dominated have different dynamics than in the unmagnetized case and that magnetic plasmas can generate strong and collimated electromagnetic emission. We therefore generalize the physical regimes of matter and electromagnetic fields around coalescing black holes that can lead to potentially detectable emission.

We thank Tamara Bogdanovic, Bernard Kelly, Carlos Palenzuela, Jeremy Schnittman, and Roman Shcherbakov for

REFERENCES

Anderson, M., Lehner, L., Megevand, M., & Neilsen, D. 2010, Phys. Rev. D, 81, 044004
Ansorg, M., Brügmann, B., & Tichy, W. 2004, Phys. Rev. D, 70, 064011
Antón, L., Zanotti, O., Miralles, J. A., et al. 2006, Astrophys. J., 637, 296
Arun, K. G., Mishra, C. K., Van Den Broeck, C., et al. 2009, Classical and Quantum Gravity, 26, 094021
Berti, E., Buonanno, A., & Will, C. M. 2005, Classical and Quantum Gravity, 22, 943
Bode, T., Bogdanovic, T., Haas, R., et al. 2012, ApJ, 744, 45
Bode, T., Haas, R., Bogdanović, T., Laguna, P., & Shoemaker, D. 2010, ApJ, 715, 1117
Bogdanović, T., Bode, T., Haas, R., Laguna, P., & Shoemaker, D. 2011, Classical and Quantum Gravity, 28, 094020
Colella, P., & Woodward, P. R. 1984, J. Comput. Phys., 54, 174
Corrales, L. R., Haiman, Z., & MacFadyen, A. 2010, MNRAS, 404, 947
Etienne, Z. B., Paschalidis, V., Liu, Y. T., & Shapiro, S. L. 2012, Phys. Rev. D, 85, 024013
Farris, B. D., Liu, Y. T., & Shapiro, S. L. 2010, Phys. Rev. D, 81, 084008
Farris, B. D., Liu, Y. T., & Shapiro, S. L. 2011, Phys. Rev. D, 84, 024024
Giacomazzo, B., & Rezzolla, L. 2006, Journal of Fluid Mechanics, 562, 223
Giacomazzo, B., & Rezzolla, L. 2007, Class. Quantum Grav., 24, S235
Giacomazzo, B., Rezzolla, L., & Baiotti, L. 2009, Mon. Not. R. Astron. Soc., 399, L164
Giacomazzo, B., Rezzolla, L., & Baiotti, L. 2011, Phys. Rev. D, 83, 044014
Harten, A., Lax, P. D., & van Leer, B. 1983, SIAM Rev., 25, 35
Hughes, S. A., & Holz, D. E. 2003, Classical and Quantum Gravity, 20, 65
Ichimaru, S. 1977, ApJ, 214, 840
Kocsis, B., Frei, Z., Haiman, Z., & Menou, K. 2006, ApJ, 637, 27
Kocsis, B., & Loeb, A. 2008, Physical Review Letters, 101, 041101
Krolik, J. H. 2010, ApJ, 709, 774
Lippai, Z., Frei, Z., & Haiman, Z. 2008, ApJ, 676, L5
Löffler, F., Faber, J., Bentivegna, E., et al. 2011, arXiv:1111.3344
Megevand, M., Anderson, M., Frank, J., et al. 2009, Phys. Rev. D, 80, 024012
Milosavljević, M., & Phinney, E. S. 2005, ApJ, 622, L93
Mizuno, Y., Zhang, B., Giacomazzo, B., et al. 2009, ApJ, 690, L47
Mösta, P., Palenzuela, C., Rezzolla, L., et al. 2010, Phys. Rev. D, 81, 064017
Mösta, P., Alic, D., Rezzolla, L., Zanotti, O., & Palenzuela, C. 2011, arXiv:1109.1177
O'Neill, S. M., Miller, M. C., Bogdanović, T., Reynolds, C. S., & Schnittman, J. D. 2009, ApJ, 700, 859
Palenzuela, C., Anderson, M., Lehner, L., Liebling, S. L., & Neilsen, D. 2009, Physical Review Letters, 103, 081101
Palenzuela, C., Garrett, T., Lehner, L., & Liebling, S. L. 2010a, Phys. Rev. D, 82, 044045
Palenzuela, C., Lehner, L., & Liebling, S. L. 2010b, Science, 329, 927
Palenzuela, C., Lehner, L., & Yoshida, S. 2010c, Phys. Rev. D, 81, 084007
Pollney, D., Reisswig, C., Rezzolla, L., et al. 2007, Phys. Rev. D, 76, 124002
Rezzolla, L., Giacomazzo, B., Baiotti, L., et al. 2011, ApJ, 732, L6
Rossi, E. M., Lodato, G., Armitage, P. J., Pringle, J. E., & King, A. R. 2010, MNRAS, 401, 2021
Schnetter, E., Hawley, S. H., & Hawke, I. 2004, Class. Quantum Grav., 21, 1465
Schnittman, J. D., & Krolik, J. H. 2008, ApJ, 684, 835
Schutz, B. F. 2009, Classical and Quantum Gravity, 26, 094020
Shapiro, S. L. 2010, Phys. Rev. D, 81, 024019
Shields, G. A., & Bonning, E. W. 2008, ApJ, 682, 758
Tanaka, T., & Menou, K. 2010, ApJ, 714, 404

Thornburg, J. 2004, Class. Quantum Grav., 21, 743

Toth, G. 2000, J. Comput. Phys., 161, 605

van Meter, J. R., Baker, J. G., Koppitz, M., & Choi, D.-I. 2006, Phys. Rev. D, 73, 124011

van Meter, J. R., Wise, J. H., Miller, M. C., et al. 2010, ApJ, 711, L89

Zanotti, O., Rezzolla, L., Del Zanna, L., & Palenzuela, C. 2010, A&A, 523, A8